ICAS 2016
30th Congress of the International Council of the Aeronautical Sciences
DCC, Daejeon, Korea ; September 25-30, 2016

EXTENDED VALIDATION OF A TRANSONIC LATTICE-BOLTZMANN METHOD ON THE EXAMPLE OF THE NASA COMMON RESEARCH MODEL

Benedikt König, André F. P. Ribeiro, Ehab Fares
Exa GmbH, Stuttgart, Germany

Raoyang Zhang, Pardeep Gopalakrishnan, Yanbing Li
Exa Corporation, Burlington, MA, USA

Abstract

A novel transonic Lattice-Boltzmann method is used to simulate the unsteady flow of a generic aircraft configuration in cruise conditions. A grid convergence study is performed and simulation results at lower angle of attack are compared to experiments. The effects of wing twist and presence of a model support sting in the wind tunnel model are evaluated. Simulations are executed also at high angles of attack in the buffet regime. Numerical results compare favorably with experimental findings and confirm the importance of an accurate representation of the geometry to achieve same flow conditions measured in the wind tunnel. The buffet phenomena are well captured and the first results are very promising.

1 Introduction

The NASA Common Research Model (CRM) [1] was developed for the AIAA Drag Prediction Workshop series and is a publicly available model representative of a contemporary transonic transport aircraft. It currently serves as a standard generic test case for Computational Fluid Dynamics (CFD) code validation and benchmarking. The Lattice-Boltzmann Method (LBM) employed in this work is an extension of the commercial PowerFLOW code, offering a new capability to simulate transonic and supersonic flows [2].

LBM in general is an alternative approach to CFD to the conventional solvers based on the numerical solution of the Navier-Stokes (N-S) equations. The LBM can be treated as a discrete form of the Boltzmann equation and it is physically motivated by the microscopic particle nature of a fluid, where the physics are more simple and general [3], recovering the N-S equations at the continuum level. The LBM approach offers several advantages over traditional CFD approaches such as effortless complex geometry handling and good performance on large computer clusters. Until recently, the commonly used D3Q19 LBM model was limited to the low subsonic flow regime, restricting its applications in the aerospace field. This restriction has been removed through some recent developments [2][4][5]. The new transonic capability is currently being validated against a number of representative test cases. In this work, the focus is on the CRM.

The CRM was used as a reference test case for the fourth, fifth, and sixth AIAA Drag Prediction Workshops (DPW) and also the first and second Aerodynamic Prediction Challenge (APC), organized by JAXA. A large number of CFD simulations were conducted, representing the state-of-the-art of the current technology [9][10].

Due to two main effects in the wind tunnel measurements, the presence of the sting support and the aeroelastic wing deformation, the overall agreement of the early CFD simulations to the experiments was indicating large discrepancies. It was documented [11] that the agreement can be improved significantly if those two effects are included in the numerical model.

In this study, the validation of the transonic LBM method is performed by comparison to wind tunnel measurements. A short summary of the numerical method is presented in section 2. Section 3 contains a description of the test case itself. The validation work done for the DPW-6, including a grid convergence study for the CRM is presented in section 4.1. Results including both the sting support geometry and the wing twist distributions measured during the experiments are shown in section 4.2. Transonic buffet results validated against the APC-II experiments are shown in section 4.3. The conclusions of the study are described in section 5.

2 Numerical method

LBM is based on the time evolution of the particle density distribution. From those discrete distribution functions, the macroscopic quantities for density, momentum and higher order moments can be obtained through simple arithmetic. The dynamics of a fluid thereby consist of two steps, namely the propagation from one lattice cell to another and the collision of the particles within one cell. This process is inherently unsteady and efficiently parallelized, with low numerical dissipation in the system. The effect of turbulence in PowerFLOW is accounted for with LBM-Very Large-Eddy Simulation (LBM-VLES) and relies on a variant of the RNG k-ε model [6] in coarser grid regions. In finer grid regions, a large part of the turbulence spectra is directly resolved. This approach makes LBM-VLES conceptually similar to hybrid RANS/LES methods. Recent developments [4],[5] of the core LBM solver allowed the extension of strong compressibility and shock effects, thus increasing the range of Mach number that can be accurately simulated up to ~2.0.

The volume grid depicted in Fig. 1 used for the simulation is based on an automatically generated Cartesian mesh and can be easily adapted through global and local refinement regions.

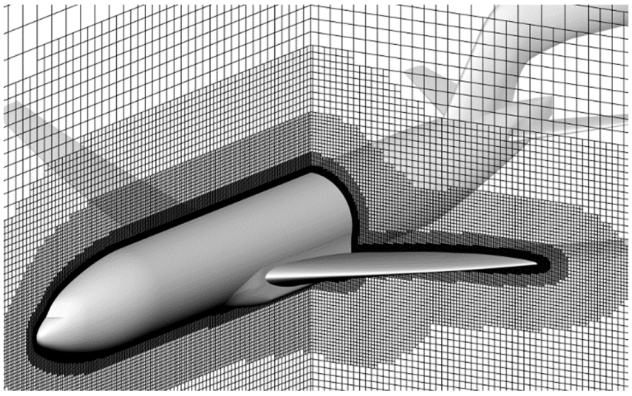

Fig. 1 Automatically generated volumetric Cartesian grid

3 Test case description

The CRM was developed by Vassberg et al. [1] specifically as a model for CFD validation. It features a modern transonic supercritical wing for a cruise Mach number of $M = 0.85$ at a design lift coefficient of $C_L = 0.5$. Several configurations are available, including a simple wing-body and a wing-body-pylon-nacelle, where the flow-through engine is installed on the wing. Cases with and without horizontal tail plane are also available. The study here will focus on the wing-body configuration (WB), wing-body-tail with zero trim configuration (WBT0), and wing-body-pylon-nacelle configuration (WBPN). The model was installed and tested in several wind tunnels including the NASA Langley National Transonic Facility (NTF) and the European Transonic Wind Tunnel (ETW) as depicted in Fig. 2. Both the NTF and ETW can operate under pressurized

cryogenic conditions to achieve flight Reynolds numbers. The results used in this work were measured at a Mach number of 0.85 and a sub-scale Reynolds numbers of $5x10^6$.

Fig. 2 CRM configuration in the ETW wind tunnel showing model and blade sting support

Another recent test campaign was conducted at the transonic wind tunnel of JAXA (JTWT) at a Reynolds number of $1.5x10^6$ which is focused on the high angle of attack unsteady flow and transonic buffet cases.

4 Simulation results

Aerodynamic results from a number of studies on the CRM are presented in the following sections.

4.1 Grid convergence study

A grid convergence study for configurations 1 and 2 of the CRM (WB and WBNP) was conducted in the context of DPW-6. Flow conditions were $Re=5x10^6$ and M=0.85. Due to the inherently time-accurate nature of the numerical method, simulations at constant angle of attack of $\alpha=2.75°$ were performed instead of the target-lift simulations, in order to reduce the computational cost. A series of five resolutions with a refinement ratio of 1.5 in total grid size, corresponding to 1.15 in linear resolution, were simulated. To account for the non-constant lift coefficient (C_L) caused by the fixed angle of attack for the two configurations, all drag coefficient (C_D) results were corrected for the lift-dependent drag using

$$C_{D,\mathrm{corr}} = C_D - \frac{0.5^2 - C_L^2}{\pi\Lambda}$$

where Λ is the aspect-ratio.

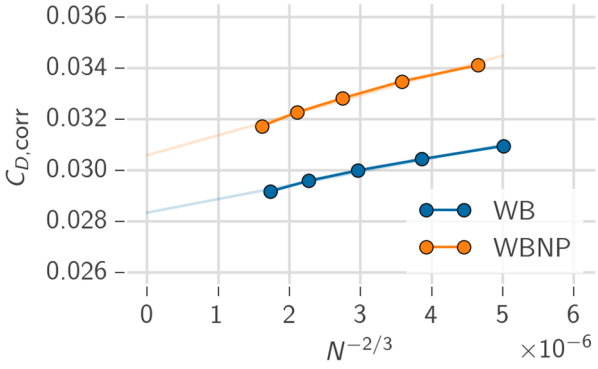

Fig. 3 Grid Convergence for configurations WB and WBNP

The corrected drag convergence is shown in the typical style used in the DPW series in Fig. 3, where N is the number of elements in the simulation domain. Drag is showing a clear convergence trend, albeit with a large variation with resolution. Trend lines for both configurations indicate that the continuum-extrapolated drag difference between the configurations is 22.5 drag counts, which is in very good agreement with the experimental value. The linear behaviour of the grid convergence also indicates a second order accuracy of the numerical scheme.

4. Wing deformation and sting effects

From deformation measurements done during the wind tunnel tests at NTF [12] and ETW [13] as well as from work by Rivers [11] it is known that the aeroelastic model deformations under load and the presence of the model support system had a non-negligible effect on the measurements. Lift is mostly impacted by the differences in the wing twist distribution due to the static aeroelastic

deformations, while drag showes the greatest sensitivity to the modeling of the sting support system.

To reproduce this finding, simulations of three different configurations were conducted for M=0.85, α=2.9° and Re=5x10^6. The angle of attack of α=2.9° corresponds to the condition where the design lift coefficient of C_L=0.5 was measured in ETW. Firstly, the baseline geometry WBT0 from the DPW series was used. Secondly, the same geometry was updated with the twist distribution of the main wing measured in ETW at α=3°. The third geometry also included the modified twist distribution but modeled the sting support system too, as shown in Fig. 4. More details on that study can be found in [14].

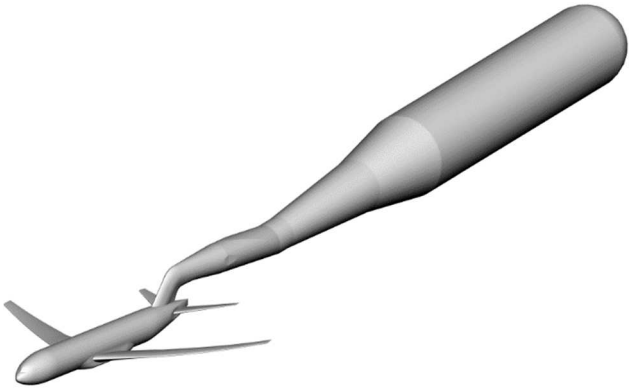

Fig. 4 Illustration of the CRM WBT0 configuration including blade sting support.

Lift and drag results for the three configurations are presented in Fig. 5 as a function of the angle of attack (α). They confirm the trends shown by Rivers [11]. The lift coefficient is reduced by almost 4 lift counts or 50% of the initial difference relative to the ETW measurement when the measured twist distribution is taken into account. On top of that, the modeling of the support sting only reduces the difference on lift by an additional 22%. In total, correction of the wing twist and including the support sting in the simulation reduces the initial deviation by 72%. Similar significant improvements can be achieved with regard to drag.

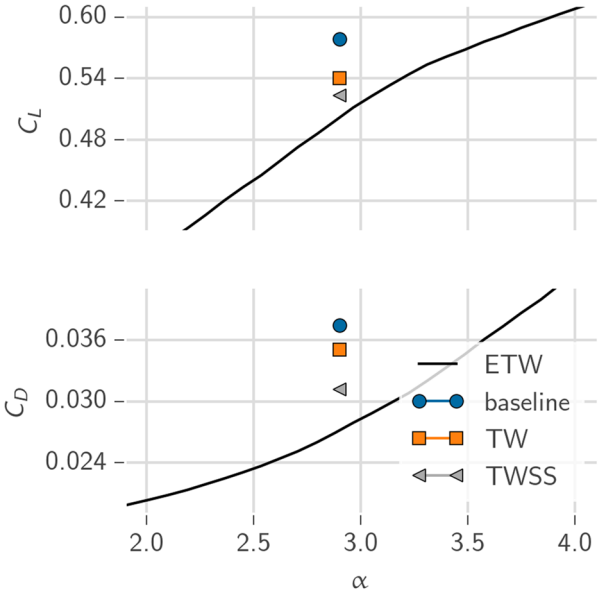

Fig. 5 Impact of wing twist distribution (TW) and model sting support (TWSS) on lift and drag.

The pressure coefficient (C_p) distribution confirms that including twist and support effects improves the agreement with experiments dramatically. Fig. 6 shows a comparison of the three configurations to experimental C_p distributions over the chord (c). It can be seen that for the inboard section at wing span percentage η=0.283 the differences between the three simulations compared to the experiments are relatively small. Here the change in twist relative to the baseline is small and only the velocity gradient introduced by the model sting support has a minor effect on the shock location.

Going further outboard it can be seen how the differences between the three configurations increase. It is interesting to note that the difference in wing twist, going from the baseline to the twist corrected model, shows the clear effect of a reduction of the local angle of attack towards the wing tip. Going outboard, the rooftop level of the pressure distributions gets more and more reduced, which is consistent with lower local angles of attack. The effect of the sting, however, is of a different nature. The suction peaks and rooftop levels are only slightly

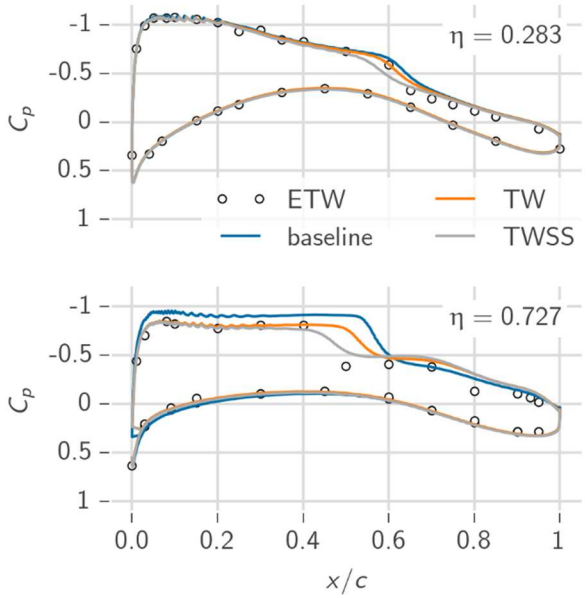

Fig. 6 Impact of wing twist distribution (TW) and sting support (TWSS) on the wing pressure distributions.

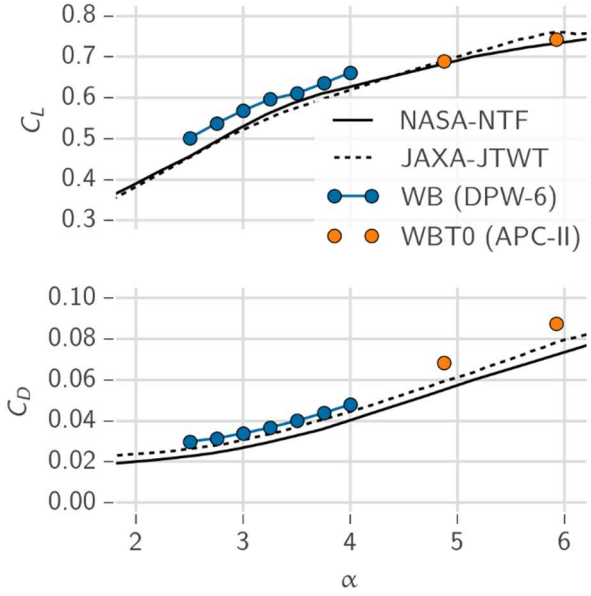

Fig. 7 Lift and drag polars including aeroelastic wing deformations for the two configurations used at the DPW-6 and the APC-II workshops, WB (Re=5x10^6) and WBT0 (Re=1.5x10^6).

affected, but the shock position moves further upstream. This indicates a local reduction in effective Mach number of the oncoming flow. Comparing the pressure distributions on the outboard wing, i.e. at η=0.727, one can see that only the inclusion of both the corrected twist and the sting support in the simulations yields a reasonable agreement to experiments.

In response to two recent workshops, DPW-6 [7] and APC-II [8], a number of simulations were done using individually adjusted wing twist distributions for each angle of attack. The model sting support was not taken into account in those studies. Lift and drag comparisons for those results are shown in Fig. 7, together with two sets of experimental results.

For the DPW-6 simulations, the WB configuration consisting of wing and fuselage only was used at a Reynolds number of Re=5x10^6, corresponding to the measurements from the NASA-NTF wind tunnel. The WBT0 configuration with an additional horizontal tail set a 0° deflection angle was run at Re=1.5x10^6 for the APC-II workshop, corresponding to the JAXA wind tunnel test of the CRM in the JTWT facility.

Generally, Fig. 7 shows that the trends of the polar are captured well by the simulations. There is some over-prediction of both lift and drag in the linear range of the polar. This is in line with the findings shown in Fig. 5 where including the sting support reduced the lift towards the measured values. However, this installation effect may not be sufficient to fully reproduce the measurements. Some discrepancies exist at the end of the linear range around buffet onset. From Fig. 9, showing standard deviation C_p (C_p') at a section in the middle of the wing, it can be seen that for angles-of-attack above α=3.25° the flow suddenly becomes very unsteady. The peak around 50% of the chord in Fig. 9 thereby represents the movement of the shock in buffet and the high fluctuations downstream of that indicate the separated flow region aft of the moving shock.

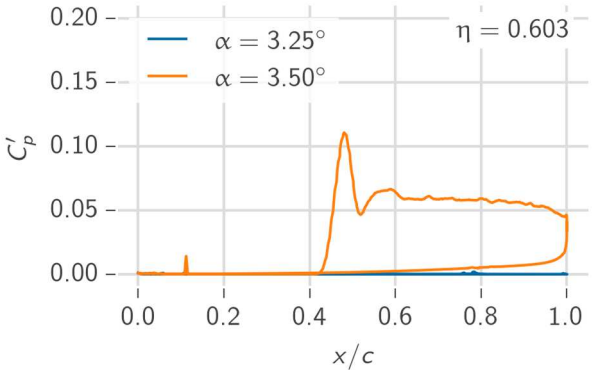

Fig. 9 Standard deviation C_p at a mid-board section for angles-of-attack α=3.25° and 3.5°.

For the two highest angles-of-attack shown in Fig. 7, which are deep in the buffet range, the agreement to experimental results is very good. A further discussion of the results under buffet conditions is presented in the following section.

4.3 Buffet results

For higher angles of attack, the CRM displays transonic buffet. This was measured experimentally by JAXA and made available for the APC-II workshop. Transonic buffet occurs when the shock strength leads to a separation on the downwind part of the wing, which in turn moves the shock upwind, making it weaker and, hence, reducing the separation. This repeats periodically and leads to aerodynamic degradation and significant structural stress on the wing. Fig. 8 shows mean C_p over the chord at

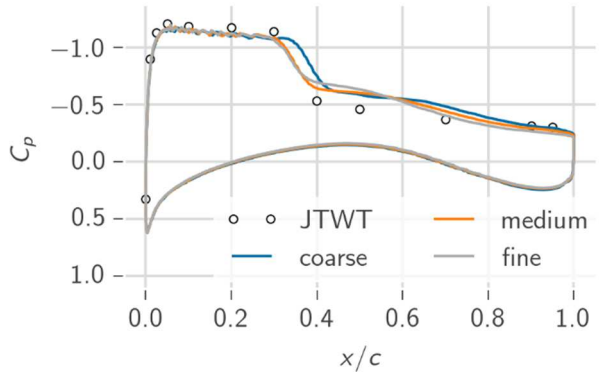

Fig. 8 Pressure distribution under buffet condition at α=4.87°.

half span for an angle of attack of 4.87° and for three resolutions different by a linear factor of 1.15[2]. The shock position is well captured and the smooth slope at the shock average position indicates it is moving back and forward along the chord. The coarse resolution results in a shock that is too far downwind compared to experiments, but the medium and fine resolution are very close together, indicating that the mesh refinement is approaching a converged result.

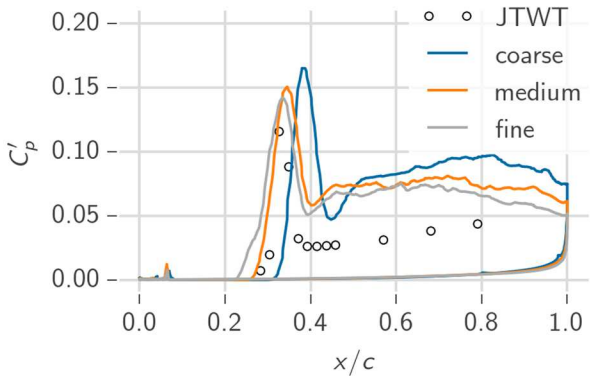

Fig. 10 Standard deviation C_p under buffet conditions at α=4.87°.

Fig. 10 shows C_p' over the chord at the same spanwise position. The peak value agrees reasonably well with the experiments and the spread of the peak, representing the region where the shock is moving, is also well captured. Consistent with mean C_p, the coarse results are displaying a shock that is too far downwind, while the medium and fine results are similar. In the second half of the chord, where the flow is fully separated, the fluctuations seem larger compared to the wind tunnel. This could be caused by insufficient mesh refinement to resolve small turbulence structures that are less coherent and energetic than the large scale structures. This would explain the reduction of levels with mesh refinement.

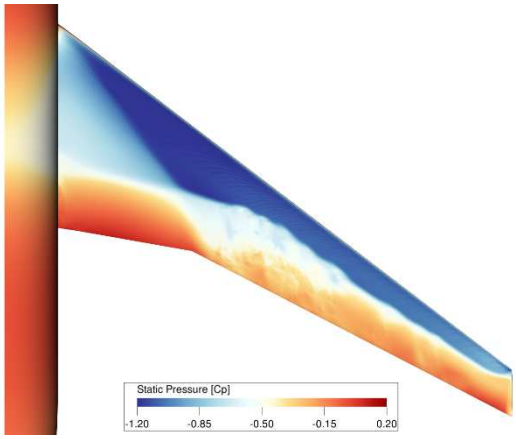

Fig. 11 Snapshot of surface C_p under buffet conditions at α=4.87°.

It is also interesting to observe that the buffet phenomenon is highly three-dimensional. A snapshot of the pressure distribution on the surface as depicted in Fig. 11 clearly shows the spanwise variation and indicate the amount of fluctuation of the shock position from mid span to tip. The buffet phenomenon will be studied in depth and compared in detail to available unsteady measurements in a subsequent investigation.

5 Conclusions

Unsteady flow simulations using the transonic Lattice-Boltzmann approach based solver PowerFLOW were conducted on several configurations of the CRM at several conditions. The grid convergence study for both low and high angles-of-attack indicate good grid convergence of second order accuracy towards the experiment. The effect of sting support and wing twist clearly emphasize the importance of an accurate representation of the model aeroelastic deformation as well as the full wind tunnel installation in order to improve the comparison with experimentally measured forces and pressure distributions. The newly developed transonic Lattice-Boltzmann based approach was able to accurately capture the flow for the various conditions and configurations and is in line with other available simulations performed by other groups at the DPW-6.

The current buffet results are very promising, showing that LBM-VLES approach is capable of simulating this challenging phenomenon. Future work will be done to perform further validation on transonic buffet.

References

[1] Vassberg J., Dehaan M., Rivers M. and Wahls R., "Development of a Common Research Model for Applied CFD Validation Studies," *26th AIAA Applied Aerodynamics Conference*, Honolulu, AIAA Paper 2008-6919, 2008.

[2] Fares E., Wessels M., Li Y., Gopalakrishnan P., Zhang R., Sun C., Gopalaswamy N., Roberts P., Hoch J. and Chen H., „Validation of a Lattice-Boltzmann Approach for Transonic and Supersonic Flow Simulations," *52nd Aerospace Sciences Meeting*, Maryland, AIAA-Paper 2014-0952, 2014.

[3] Chen H., „Volumetric Formulation of the Lattice-Boltzmann Method for Fluid Dynamics: Basic Concept," *Physical Review E*, Vol. 58, No. 3, pp 3955-3963, 1998.

[4] Shan X., Yuan X.F. and Chen H., „Kinetic theory representation of hydrodynamics: a way beyond the Navier–Stokes equation," *Journal of Fluid Mechanics*, Vol. 550, pp 413- 441, March 2006.

[5] Zhang R., Shan X. and Chen H., „Efficient kinetic method for fluid simulation beyond the Navier-Stokes equation," *Physical Review E*, Vol. 74, pp 046703, , 2006.

[6] Yakhot V., Orszag S.A:, Thangam S., Gatski T.B. and Speziale C.G., „Development of Turbulence Models for Shear Flows by a Double Expansion Technique," *Physics of Fluids A*, Vol. 4, No.. 7, pp 1510–1520, 1992.

[7] 6th AIAA CFD Drag Prediction Workshop, http://aiaa-dpw.larc.nasa.gov/, retrived June 2016

[8] Second Aerodynamics Prediction Challenge (APC-II), https://cfdws.chofu.jaxa.jp/apc/, retrived June 2016

[9] Vassberg J.C., Tinoco E.N., Mani M., Rider B., Zickuhr T., Levy D.W., Brodersen O.P., Eisfeld B., Crippa S., Wahls R.A., Morrison J.H., Mavriplis D.J. and Murayama M., „Summary of the Fourth AIAA CFD Drag Prediction Workshop," *Journal of Aircraft,* Vol. 51, No. 4, pp 1070-1089, 2014.

[10] Levy D.W., Laflin K.R., Tinoco E.N., Vassberg J.C., Mani M., Rider B., Rumsey C.L., Wahls R.A.,

Morrison J.H., Brodersen O.P., Crippa S., Mavriplis D.J. and Murayama M, „Summary of Data from the Fifth AIAA CFD Drag Prediction Workshop," *51st AIAA Aerospace Sciences Meeting*, Grapevine, AIAA-Paper 2013-0046, 2013.

[11] Rivers M.B., Hunter C.A and Campbell E.L., "Further Investigation of the Support System Effects and Wing Twist on the NASA Common Research Mode," *30th AIAA Applied Aerodynamics Conference*, New Orelans, AIAA-Paper 2012-3209, 2012.

[12] Melissa Rivers, NASA Common Research Model, http://commonresearchmodel.larc.nasa.gov/, accessed June 2016

[13] European Strategic Wind tunnels Improved Research Potential (ESWIRP), http://www.eswirp.eu/ETW-TNA-Dissemination.html, The ESWIRP ETW TNA test results, accessed June 2016

[14] König B., Fares, E. Validation of a Transonic Lattice-Boltzmann Method on the NASA Common Research Model, *54th AIAA Aerospace Sciences Meeting*, AIAA Paper 2016-2023, 2016

Contact Author Email Address

benedikt@exa.com

Copyright Statement